INTERNATIONAL JOURNAL FOR NUMERICAL METHODS IN FLUIDS
Int. J. Numer. Meth. Fluids 2009; **59**:1351–1368
Published online 31 July 2008 in Wiley InterScience (www.interscience.wiley.com). DOI: 10.1002/fld.1870

Effect of magnetic Reynolds number on the two-dimensional hydromagnetic flow around a cylinder

T. V. S. Sekhar[1,*,†], R. Sivakumar[2] and T. V. R. Ravi Kumar[3]

[1]*Department of Mathematics, Pondicherry Engineering College, Puducherry 605014, India*
[2]*Department of Physics, Pondicherry University, Puducherry 605014, India*
[3]*Department of Applied Mathematics, Ideal College of Arts and Sciences, Kakinada 533003, India*

SUMMARY

Numerical experiments have been conducted to study the effect of magnetic Reynolds number on the steady, two-dimensional, viscous, incompressible and electrically conducting flow around a circular cylinder. Besides usual Reynolds number Re, the flow is governed by the magnetic Reynolds number R_m and Alfvén number β. The flow and magnetic field are uniform and parallel at large distances from the cylinder. The pressure Poisson equation is solved to find the pressure fields in the entire flow region. The effects of the magnetic field and electrical conductivity on the recirculation bubble, drag coefficient, standing vortex and pressure are presented and discussed. For low interaction parameter ($N<1$), the suppression of the flow-separation is nearly independent of the conductivity of the fluid, whereas for large interaction parameters, the conductivity of the fluid strongly influences the control of flow-separation. Copyright © 2008 John Wiley & Sons, Ltd.

Received 1 November 2007; Revised 26 March 2008; Accepted 25 May 2008

KEY WORDS: magnetic Reynolds number; flow-separation; flow control; magnetohydrodynamics; drag coefficient; full MHD

1. INTRODUCTION

Magnetic fields are employed in problems related to melting, levitating, stabilizing liquid metals, growing semiconductor single crystals, reducing drag in duct flows, designing fusion reactors, flow-controls for hypersonic vehicles and in controlling turbulence and in nanofluditics. Depending on the application, the magnetic Reynolds number R_m can vary dramatically. For instance, in two-dimensional steady magneto-aerodynamics, R_m of the order of unity is permissible [1]. In astrophysical problems, R_m can be extremely high, of the order 10^2–10^6. On the contrary, for flows involving liquid metals and semiconductors it will vary over a wide range 10^{-5}–1. An interesting

*Correspondence to: T. V. S. Sekhar, Department of Mathematics, Pondicherry Engineering College, Puducherry 605014, India.
†E-mail: sekhartvs@yahoo.co.in

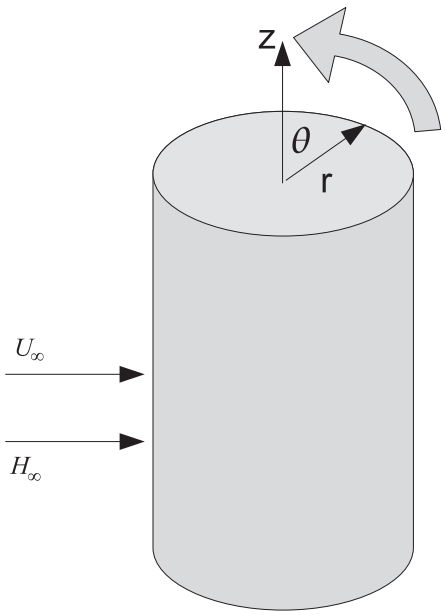

Figure 1. Schematic representation of the flow configuration.

area where R_m is small is electrokinetics-based microfluidics where convenient and efficient mechanisms for manipulating and controlling liquid flows in micro-devices are needed. Modelling and understanding fluid flows in microscale geometry, especially in microchannels, are important in the design and control of various micro-electromechanical systems and many other instruments used in modern technology. It has been appreciated that combined electromagnetohydrodynamic effects can potentially be utilized to enhance the liquid flow rates in microchannels. Experimentally, it has been shown [2] that the average flow rates in micropumps can be substantially augmented by employing low magnetic fields. Recently, the influence of electromagnetic fields on the surface tension-driven flow in a parallel plate microchannel under the assumption of *negligible* magnetic Reynolds number has been analyzed [3]. For low values of R_m, the cylinder wake control and their instabilities in an external magnetic field have been studied [4] and the non-monotonic behavior of the cylinder wake using vorticity-streamfunction formulation is observed at low, moderate and high Reynolds numbers [5–7]. In any case, at low or negligible values of R_m, when an external magnetic field is present, it is customary to make use of the so-called quasi-static (QS) approximation. In this approximation, induced magnetic fluctuations are much smaller than the applied magnetic field and the overall magnetic effect amounts to adding in the Navier–Stokes equations an extra damping term, which affects only Fourier modes having a component parallel to the magnetic field. The derivation of the QS approximation involves taking the limit of vanishing R_m and hence its domain of validity is an interesting question. Indeed, certain applications, such as advanced schemes for the control of magnetogasdynamic flows around hypersonic vehicles, involve values of R_m of the order of 1–10 [8]. Recently, Knaepen *et al.* [9] presented the limitations of QS approximation in the magnetohydrodynamic turbulence at moderate magnetic Reynolds number in the range $0.1 \leqslant R_m \leqslant 20$.

DOI: 10.1002/fld

$$\vec{j}_1=\vec{q}_r\times\vec{h}_\theta \qquad \vec{j}_2=\vec{q}_\theta\times\vec{h}_r$$

$$\vec{F}_1=\vec{j}_1\times\vec{h}_\theta \qquad \vec{F}_2=\vec{j}_2\times\vec{h}_r$$

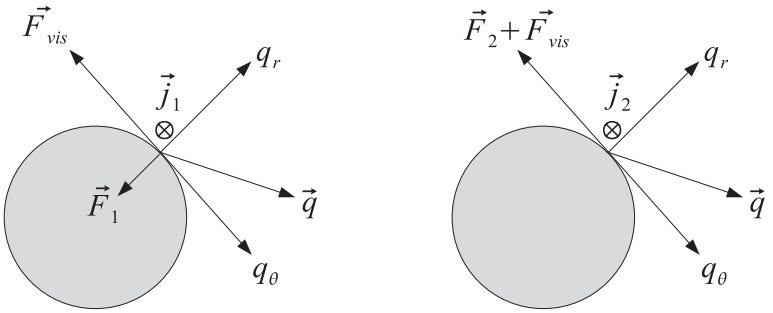

Figure 2. Schematic representation of the forces acting on the cylinder.

In essence, we have highlighted numerical and theoretical investigations on a variety of physical problems where the QS approximations are invariably used. It is known that for a fluid of extremely high conductivity, steady-state solutions do exist [10]. Recently, it is reported that with increasing Hartmann number, the difference between the solutions of the full MHD equations and low-R_m approximation increases, and in particular, for Prandtl numbers reaching lower values like those of liquid metals, this difference increases [11]. Hence, in this present study the steady flow control problem around a circular cylinder with an aligned magnetic field is considered by taking the magnetic Reynolds number into consideration (i.e. induced magnetic field) in the range $0\leqslant R_\mathrm{m}\leqslant 2$ and its effect on the flow is studied. We also compare our full MHD results with those obtained under QS approximation where possible.

2. FORMULATION OF THE PROBLEM

The equations governing the motion of an electrically conducting fluid past a circular cylinder with a uniformly applied magnetic field at large distances are, in non-dimensional form,

$$\nabla\times\mathbf{q}=\boldsymbol{\omega} \tag{1}$$

$$(\mathbf{q}\cdot\nabla)\mathbf{q}=-\nabla p+\frac{2}{Re}\nabla^2\mathbf{q}+\beta\mathbf{j}\times\mathbf{H} \tag{2}$$

$$\mathbf{j}=\nabla\times\mathbf{H}=\frac{R_\mathrm{m}}{2}[\mathbf{E}+\mathbf{q}\times\mathbf{H}] \tag{3}$$

$$\nabla\cdot\mathbf{q}=0 \tag{4}$$

DOI: 10.1002/fld

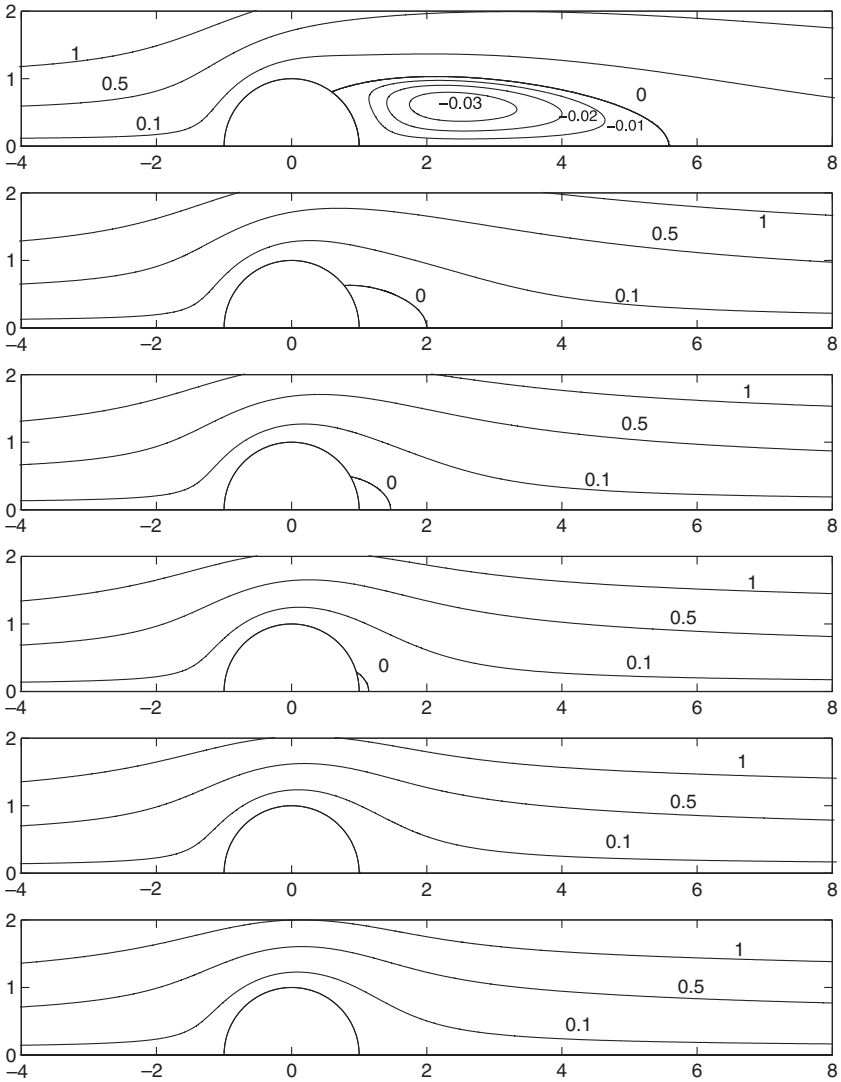

Figure 3. Streamlines for $Re=40$, $R_m=0.5$, $\beta=0$, 2, 4, 8, 12 and 16 (a–f, top to bottom).

$$\nabla\cdot\mathbf{H}=0 \tag{5}$$

$$\nabla\times\mathbf{E}=0 \tag{6}$$

where p is the pressure, $\mathbf{q}$ the fluid velocity, $\mathbf{H}$ the magnetic field, $\mathbf{E}$ the electric field, $\mathbf{j}$ the current density and $\boldsymbol{\omega}$ the vorticity. The Reynolds number is $Re=2Ua/v$ and the magnetic Reynolds number is given by $R_m=2aU\mu\sigma$. The Alfvén number β is the ratio of the square of the Alfvén speed to the square of the main stream speed. The kinematic viscosity, density, magnetic permeability and

DOI: 10.1002/fld

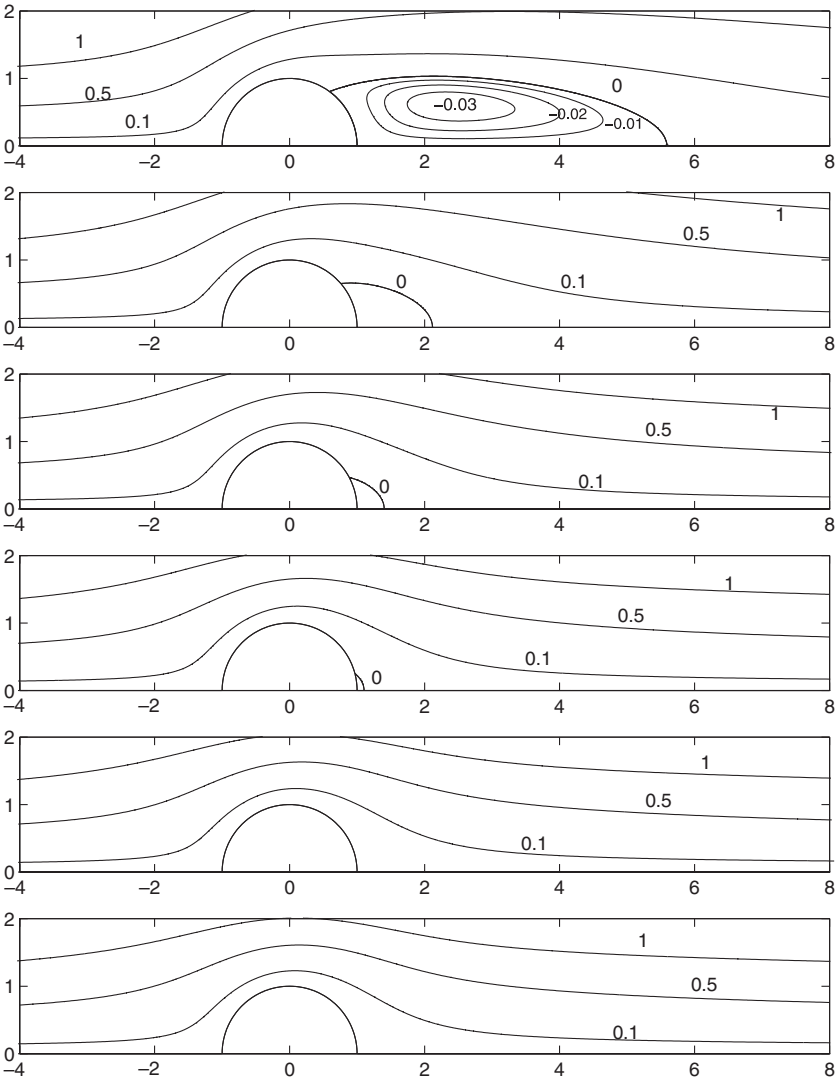

Figure 4. Streamlines for $Re = 40$, $R_m = 1$, $\beta = 0$, 1, 2, 4, 6 and 8 (a–f, top to bottom).

electrical conductivity of the fluid are ν, ρ, μ and σ, respectively. Since the flow is two dimensional, $\mathbf{E} = (0, 0, 0)$. Cylindrical polar co-ordinates (r, θ, z) are used as they are the most suitable in dealing with cylindrical boundaries. A schematic diagram showing the flow configuration is depicted in Figure 1.

The co-ordinate system is set up such that the velocity and magnetic field are parallel at large distances and the flow is symmetric, about $\theta = 0$ and 180°. In addition,

$$\mathbf{q} = (q_r, q_\theta, 0), \quad \mathbf{H} = (h_r, h_\theta, 0) \quad \text{and} \quad \mathbf{j} = (0, 0, j) \tag{7}$$

DOI: 10.1002/fld

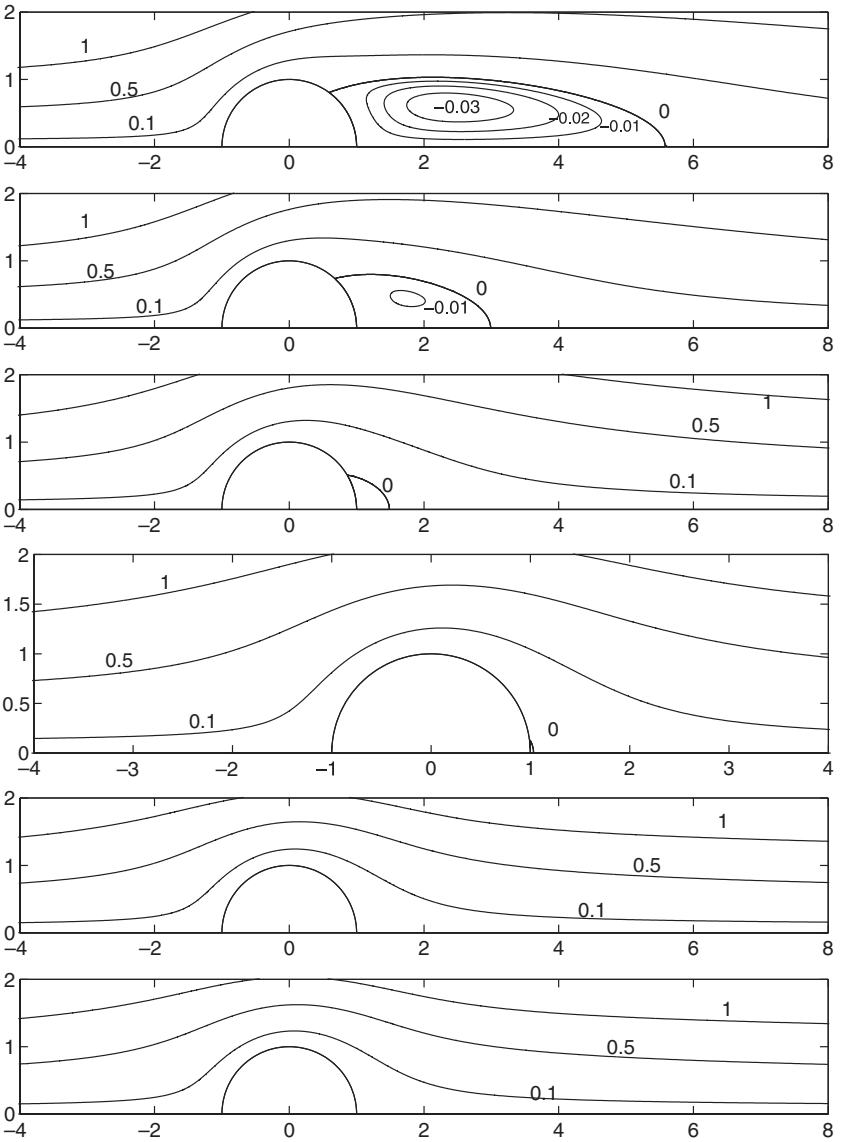

Figure 5. Streamlines for $Re=40$, $R_m=2$, $\beta=0$, 0.5, 1, 2, 3 and 4 (a–f, top to bottom).

In order to satisfy Equations (4) and (5) the dimensionless stream function $\psi(r,\theta)$ and magnetic stream function $A(r,\theta)$ are introduced such that

$$q_r=\frac{1}{r}\frac{\partial\psi}{\partial\theta},\quad q_\theta=-\frac{\partial\psi}{\partial r} \tag{8}$$

$$h_r=\frac{1}{r}\frac{\partial A}{\partial\theta},\quad h_\theta=-\frac{\partial A}{\partial r} \tag{9}$$

DOI: 10.1002/fld

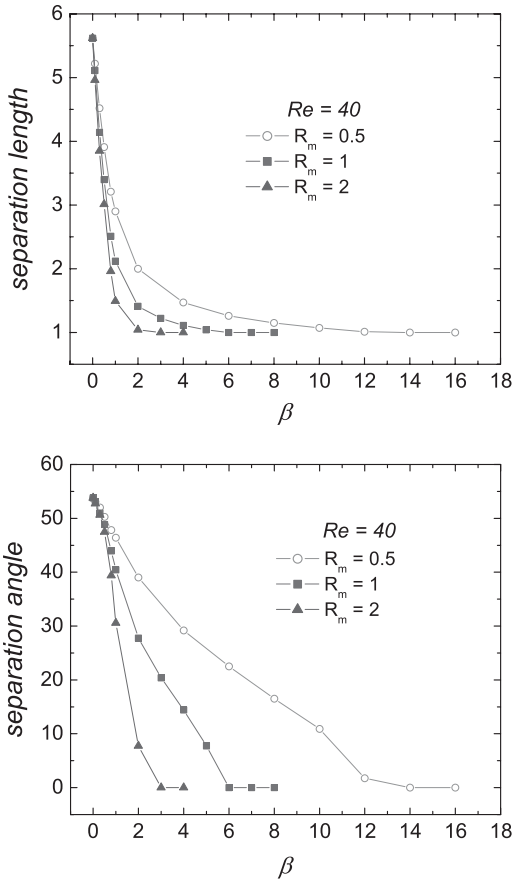

Figure 6. Dependence of separation angle θ and the separation length l on the magnetic field β.

Substitution of (7)–(9) in (1)–(3) with the transformation $r = e^{\pi\xi}$ and $\theta = \pi\eta$ yields, in the vorticity-stream function form, the following:

$$\frac{\partial^2\psi}{\partial\xi^2} + \frac{\partial^2\psi}{\partial\eta^2} + \pi^2 e^{2\pi\xi}\omega = 0 \tag{10}$$

$$\begin{aligned}
&\frac{\partial^2\omega}{\partial\xi^2} + \frac{\partial^2\omega}{\partial\eta^2} - \frac{Re}{2}\left(\frac{\partial\psi}{\partial\eta}\frac{\partial\omega}{\partial\xi} - \frac{\partial\omega}{\partial\eta}\frac{\partial\psi}{\partial\xi}\right) \\
&\quad = -\frac{e^{-2\pi\xi} Re R_m \beta}{4\pi^2}\left[-\frac{\partial\psi}{\partial\eta}\frac{\partial A}{\partial\eta}\frac{\partial^2 A}{\partial\xi^2} - \frac{\partial\psi}{\partial\xi}\frac{\partial A}{\partial\xi}\frac{\partial^2 A}{\partial\eta^2} + 2\pi\frac{\partial\psi}{\partial\eta}\frac{\partial A}{\partial\eta}\frac{\partial A}{\partial\xi} + \frac{\partial A}{\partial\xi}\frac{\partial\psi}{\partial\eta}\frac{\partial^2 A}{\partial\xi\partial\eta}\right. \\
&\qquad \left. + \frac{\partial\psi}{\partial\xi}\frac{\partial A}{\partial\eta}\frac{\partial^2 A}{\partial\xi\partial\eta} - 2\frac{\partial A}{\partial\xi}\frac{\partial A}{\partial\eta}\frac{\partial^2\psi}{\partial\xi\partial\eta} - 2\pi\frac{\partial\psi}{\partial\xi}\left(\frac{\partial A}{\partial\eta}\right)^2 + \left(\frac{\partial A}{\partial\eta}\right)^2\frac{\partial^2\psi}{\partial\xi^2} + \left(\frac{\partial A}{\partial\xi}\right)^2\frac{\partial^2\psi}{\partial\eta^2}\right]
\end{aligned} \tag{11}$$

DOI: 10.1002/fld

$$\frac{\partial^2 A}{\partial \xi^2}+\frac{\partial^2 A}{\partial \eta^2}=\frac{R_\mathrm{m}}{2}\left(\frac{\partial \psi}{\partial \eta}\frac{\partial A}{\partial \xi}-\frac{\partial \psi}{\partial \xi}\frac{\partial A}{\partial \eta}\right) \tag{12}$$

The following pressure Poisson equation that is obtained by taking divergence of Equation (2) is then solved to find the pressure in the flow field:

$$\begin{aligned}-\left(\frac{\partial^2 p}{\partial \xi^2}+\frac{\partial^2 p}{\partial \eta^2}\right)=\frac{2\mathrm{e}^{-2\pi\xi}}{\pi^2}&\left[\left(\frac{\partial^2 \psi}{\partial \xi \partial \eta}-\pi\frac{\partial \psi}{\partial \eta}\right)^2-\left(\frac{\partial^2 \psi}{\partial \xi^2}-\pi\frac{\partial \psi}{\partial \xi}\right)\left(\frac{\partial^2 \psi}{\partial \eta^2}+\pi\frac{\partial \psi}{\partial \xi}\right)\right]\\
&+\frac{ReR_\mathrm{m}\beta}{4}\frac{\mathrm{e}^{-4\pi\xi}}{\pi^4}\left[2\pi\frac{\partial \psi}{\partial \eta}\left(\frac{\partial A}{\partial \xi}\right)^2-2\frac{\partial \psi}{\partial \eta}\frac{\partial A}{\partial \xi}\frac{\partial^2 A}{\partial \xi^2}-\left(\frac{\partial A}{\partial \xi}\right)^2\frac{\partial^2 \psi}{\partial \xi \partial \eta}\right.\\
&+\left(\frac{\partial A}{\partial \eta}\right)^2\frac{\partial^2 \psi}{\partial \xi \partial \eta}+\frac{\partial \psi}{\partial \xi}\frac{\partial A}{\partial \eta}\frac{\partial^2 A}{\partial \xi^2}-2\pi\frac{\partial \psi}{\partial \xi}\frac{\partial A}{\partial \eta}\frac{\partial A}{\partial \xi}+\frac{\partial \psi}{\partial \xi}\frac{\partial A}{\partial \xi}\frac{\partial^2 A}{\partial \xi \partial \eta}-\frac{\partial \psi}{\partial \eta}\frac{\partial A}{\partial \eta}\frac{\partial^2 A}{\partial \xi \partial \eta}\\
&\left.+\frac{\partial A}{\partial \eta}\frac{\partial A}{\partial \xi}\frac{\partial^2 \psi}{\partial \xi^2}-\frac{\partial \psi}{\partial \eta}\frac{\partial A}{\partial \xi}\frac{\partial^2 A}{\partial \eta^2}-\frac{\partial \psi}{\partial \eta}\frac{\partial A}{\partial \xi}\frac{\partial^2 \psi}{\partial \eta^2}+2\frac{\partial \psi}{\partial \xi}\frac{\partial A}{\partial \eta}\frac{\partial^2 A}{\partial \eta^2}\right]\end{aligned} \tag{13}$$

2.1. Boundary conditions

Equations (10)–(12) must now be solved subject to the following boundary conditions. On the surface of the cylinder, no-slip condition is applied. At far off distances ($\xi\to\infty$) uniform flow is imposed. In order to avoid computation of magnetic field inside the cylinder, we assume that the cylinder has infinite electrical conductivity. Such assumption of using a perfectly conducting cylinder has been reported [12]. The boundary conditions applied are

- on the surface of the cylinder: $\psi=\partial\psi/\partial\xi=0, \omega=-(1/\pi^2)(\partial^2\psi/\partial\xi^2),\ A=0$;
- at large distances from the cylinder: $\psi\sim\mathrm{e}^{\pi\xi}\sin(\pi\eta), \omega\to 0,\ A\to\mathrm{e}^{\pi\xi}\sin(\pi\eta)$;
- on the axis of symmetry: $\psi=0,\ \omega=0,\ A=0$.

For Equation (13) the boundary conditions are

- on the surface of the cylinder ($\xi=0$): $\partial p/\partial\xi=-(2/Re)(\partial\omega/\partial\eta)$;
- at large distances from the cylinder ($\xi\to\infty$): $p=0$;
- along the axis of symmetry ($\eta=0, \eta=1$): $\partial p/\partial\eta=0$.

3. SOLUTION PROCEDURE

The governing partial differential equations are solved by first applying the finite difference method and the resulting algebraic equations are solved by using the multigrid method. Here, a recursive multigrid procedure is employed in which the smoother is a point Gauss–Seidel iteration and the usual coarse grid correction is applied [13, 14]. Since upwind differences are used for convective terms, the defect correction technique [13] is employed to improve the solution to second-order accuracy. Similar defect correction methods are recently being used [15, 16].

DOI: 10.1002/fld

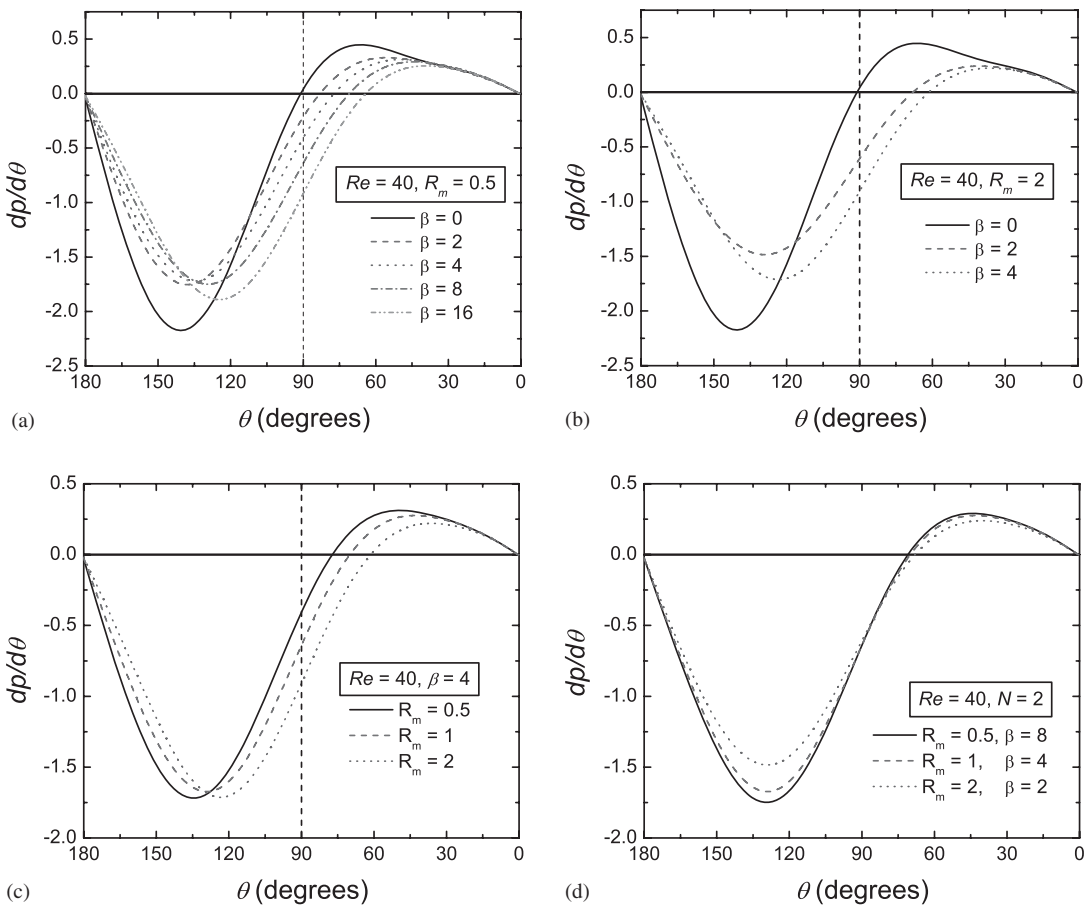

Figure 7. The variation of $\partial p/\partial\theta$ along the surface of the circular cylinder for different values of β and R_{m}.

4. RESULTS AND DISCUSSIONS

We present the results obtained for $Re=40$ and for different values of the magnetic field β and the magnetic Reynolds number R_{m}. The finest grid used here is 512×512, whereas 256×256, 128×128 are coarser grids and 64×64 is the coarsest grid. The second-order accurate solutions converged with $\varepsilon<10^{-6}$ obtained from the finest grid 512×512 are used for the discussion of the results. We have uniformly chosen 41 times the radius of cylinder as far-field distance, which is sufficiently a large domain to obtain accurate results for all values of β and R_{m}.

4.1. Recirculation bubble and adverse pressure gradient

It is customary to represent the interaction of magnetic field with the conducting fluid by the interaction parameter N, usually defined as the ratio of magnetic forces to inertial forces. If the induced magnetic field is neglected, we have the low-R_{m} approximation, in which case, N is the only

DOI: 10.1002/fld

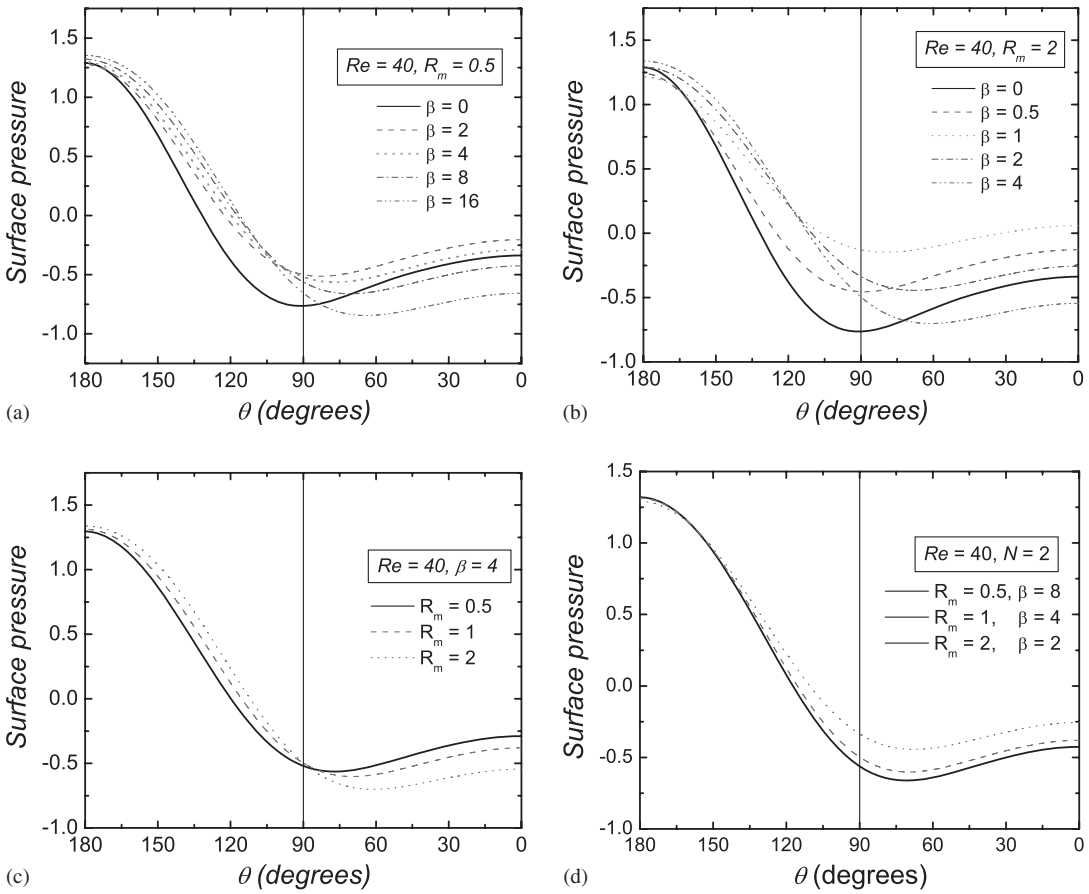

Figure 8. The angular evolution of surface pressure for various values of β and R_{m}.

parameter. In the present problem, we have two parameters (besides Re), β and R_{m}, which can be related to interaction parameter $N = 1/2R_{\mathrm{m}}\beta$. The radial and transverse components of magnetic field affect the transverse and radial components of velocity respectively. A sketch of the forces acting on the cylinder is shown in Figure 2. The effect of the magnetic field and the magnetic Reynolds number on the streamlines for $Re = 40$ are presented in Figures 3–5. From these figures, it is evident that for sufficient strength of the magnetic field, the recirculation bubble behind the circular cylinder is completely suppressed for all values of R_{m}. It is observed that for higher values of Alfven number, the flow becomes straightened in the main stream direction and the curvature of the recirculation bubble (i.e. $\psi = 0$) decreases. The flow inside the recirculation bubble slows down monotonically as the magnetic field increases. For a given applied magnetic field the suppression of the flow-separation will be more for higher values of R_{m}. Further, it is noted that, when $N < 1$, the suppression of the recirculation bubble is mainly controlled by the strength of the magnetic field, whereas when $N > 1$ the conductivity of the fluid enhances the suppression even with relatively lower magnetic field strengths (Figures 3(b), 4(b), 5(b)). The variation of the separation angle (θ_{s}) and the length of the recirculation bubble (l) with β are depicted in Figure 6.

DOI: 10.1002/fld

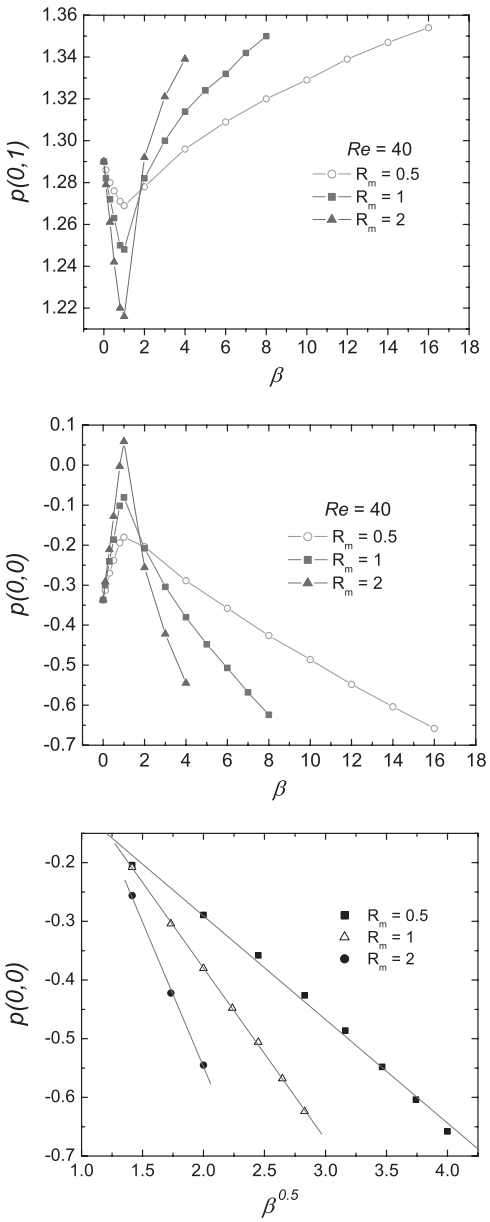

Figure 9. (Top) Pressure at front stagnation; (middle) pressure at rear stagnation point and (bottom) linear dependence of the rear pressure coefficient.

If the strength of the magnetic field is increased for a fixed R_m, the forces acting on the fluid leads to an effective reduction in magnitude of the adverse pressure gradient in the downstream region as shown in Figure 7(a) and (b). In addition, the position at which the adverse pressure

DOI: 10.1002/fld

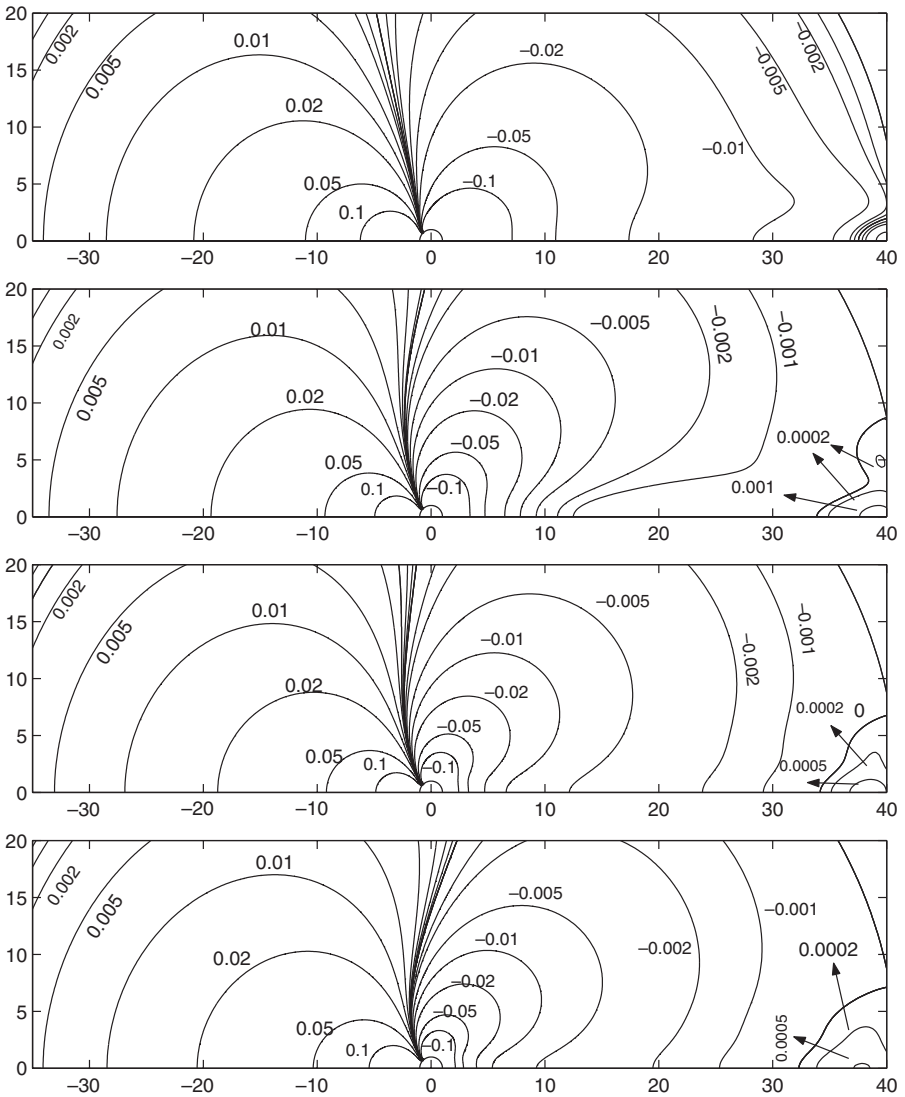

Figure 10. Isocontours of pressure for $R_m = 0.5$, $\beta = 0$, 2, 8 and 16.

gradient exists gets pushed down (towards rear stagnation point) as the magnetic field is increased and consequently the separation of the flow is delayed. However, for large magnetic fields, the magnetic field is less effective in pushing down the adverse pressure gradient downstream. The magnitudes of the adverse pressure gradient decreases with increase in strength of the magnetic field. The region of the influence of the magnetic field increases with increase in conductivity of the fluid. Further, the magnitude of adverse pressure gradient on the surface of the cylinder coincides with that of zero magnetic field case, indicating that highly conducting flows (i.e. with

DOI: 10.1002/fld

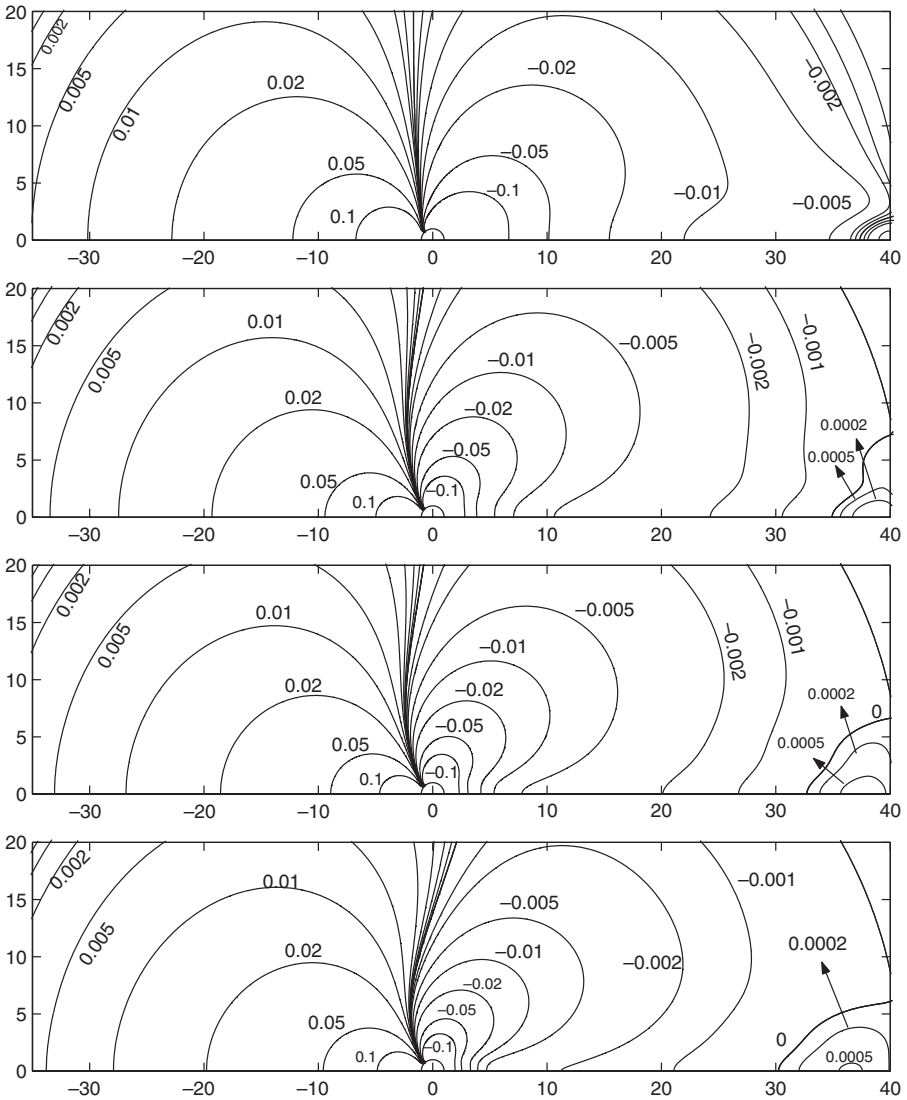

Figure 11. Isocontours of pressure for $\beta = 4$, $R_m = 0$, 0.5, 1 and 2.

higher R_m) can be stabilized with relatively low magnetic fields (Figure 7(c)). For the same strength of magnetic field, the magnitude and position of the adverse pressure gradient are reduced for highly conducting fluids, i.e. for higher values of R_m. In addition, the occurrence of the maximum adverse pressure gradient magnitude is shifted towards the rear stagnation point. For a given interaction parameter (N), the angular variation of pressure gradient is depicted in Figure 7(d). If we were to consider the low-R_m limit, the three curves in Figure 7(d) will coincide. The higher magnetic Reynolds number of the fluid effectively reduces the magnitude of the pressure gradient. It also reduces the angle at which adverse pressure gradient starts.

DOI: 10.1002/fld

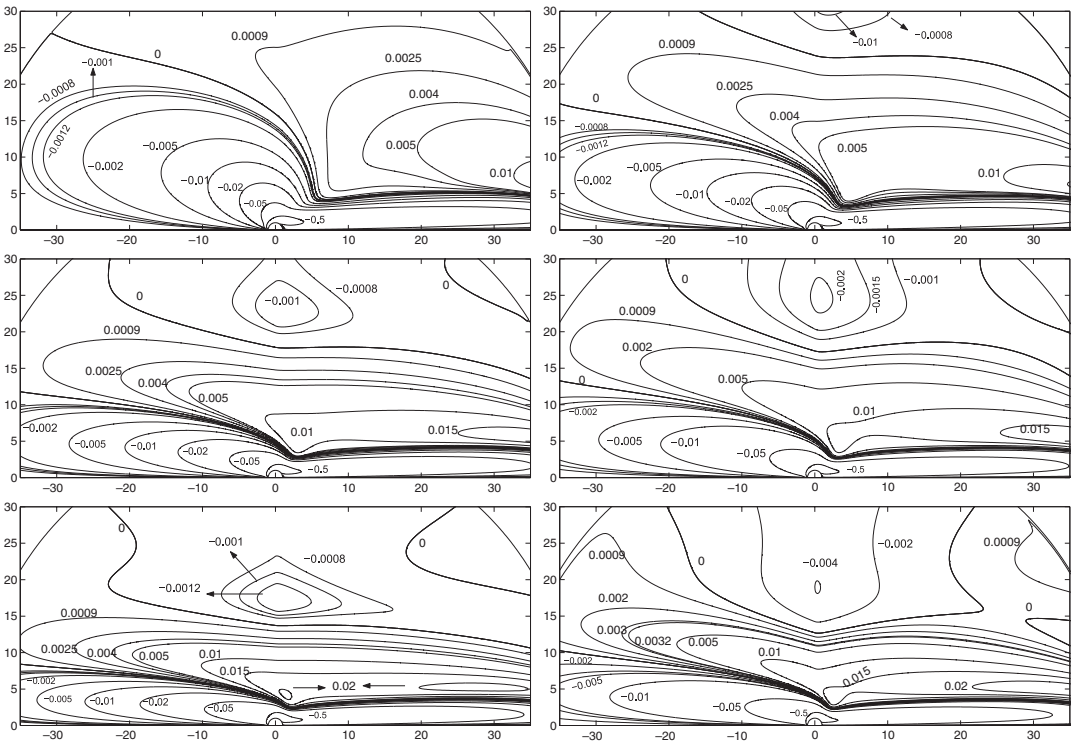

Figure 12. Isocontours of vorticity (left) $R_m = 0.5$, $\beta = 2, 8$ and 16 and (right) $\beta = 4$, $R_m = 0.5$, 1 and 2.

4.2. *Pressure fields and surface pressure*

For low values of N (less than or nearly 1), the pressure near the front stagnation point decreases. Except for this feature, the base pressure continuously increases in both the upstream and downstream regions. The latter feature has been experimentally observed by Josserand *et al.* under QS approximation. With further increase in magnetic field ($N > 1$), rear pressure inversion occurs, i.e. the upstream base pressure increases continuously, whereas downstream base pressure decreases. This is in agreement with the experimental results of Maxworthy [17] and Josserand *et al.* [18]. It is clear that a particular value of N can be obtained by different combinations of R_m and β. In Figure 8(d), the angular evolution of surface pressure for the same interaction parameter $N = 2$ is presented. In fact, the pressure near the front stagnation point decreases, whereas the pressure in the downstream region increases. It can be observed from this figure that the magnetic Reynolds number has the effect of altering the surface pressure, which, in turn, can control the flow separation. For a fixed value of β, as R_m increases (Figure 8(c)) the upstream pressure increases and the downstream pressure decreases. With regard to the magnetic field, the surface pressure at $\theta = 90^\circ$ (the interface between upstream and downstream regions) increases until $N < 1$, beyond which it decreases. This is in accordance with the experimental findings of Maxworthy [17, 19] and Yonas [20]. The pressure at front stagnation point $p(\xi = 0, \eta = 1)$ decreases until $N < 1$ and then increases. Similarly, the pressure at rear stagnation point $p(\xi = 0, \eta = 0)$ increases until $N < 1$

DOI: 10.1002/fld

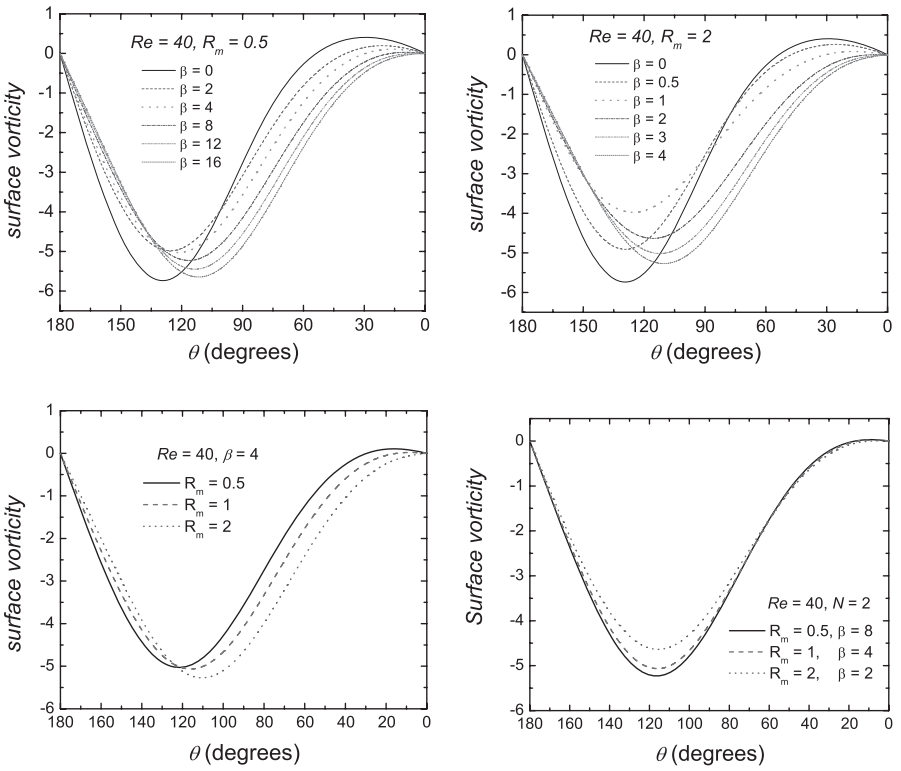

Figure 13. The angular evolution of surface vorticity for various values of β and R_{m}.

and then decreases (Figure 9). The pressure at rear stagnation point varies with $\sqrt{\beta}$ for $N>1$ (Figure 9). This feature agrees with the experimental results of Josserand *et al.* [18]. The pressure fields $p(\xi, \eta)$ in the entire flow region are presented in Figures 10 and 11. From the plots of angular evolution of surface pressure, it is observed that in comparison with the case of zero magnetic field, the increase in pressure around the front stagnation point is in line with the hypothesis of Maxworthy [17, 19] that a stagnant flow develops upstream of the cylinder when the magnetic field is increased. This feature is also observed by Josserand *et al.* [18].

4.3. Vortices

The vorticity of the fluid changes considerably with applied magnetic field due to the fact that the magnetic force is proportional to fluid velocity and resists the flow of fluid in any direction other than that of the unperturbed magnetic field near the cylinder. The length of the standing vortex is reduced slightly and the strength of the disturbance in front and rear of the cylinder is increased with increasing magnetic field. A growing inviscid rotational region (separation without flow reversal) is found, which is predicted theoretically by Leibovich [21]. Here, the word 'separation' is intended to mean an unbounded penetration of rotational fluid into the main stream [22]. These features can be seen from the vorticity contours as shown in Figure 12 for various values of β and R_{m}. It is also noted that, with increasing magnetic field or conductivity of the fluid, the region of positive

DOI: 10.1002/fld

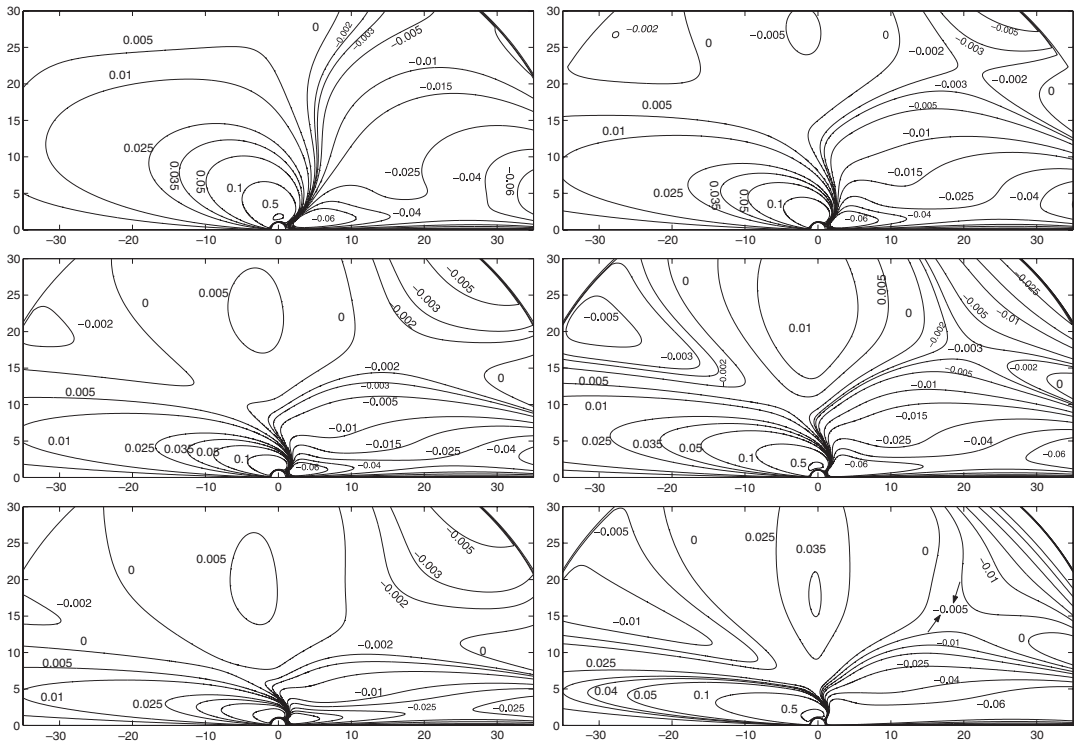

Figure 14. Isocontours of current density (left) $R_m = 0.5$, $\beta = 2$, 8 and 16 and (right) $\beta = 4$, $R_m = 0.5$, 1 and 2.

vorticity extends upstream and gets concentrated near the cylinder, whereas a negative vorticity region is again formed at far distances. The angular variation of vorticity on the surface of the cylinder is shown in Figure 13. It is clear from this figure that the magnetic field tends to destroy the surface vorticity over the cylinder and, in particular, the vorticity is destroyed to a maximum extent for $N \lesssim 1$. The contours of the current density lines are presented in Figure 14.

4.4. Drag coefficient

The variations of pressure drag coefficient (C_P), viscous drag coefficient (C_V) and total drag coefficient (C_D) with β and R_m are shown in Figure 15. When compared with the zero field case, for fluids with different conductivities, both viscous and pressure drag coefficients decrease for small magnetic fields given by $\beta \lesssim 1$. Further increase in the magnetic field leads to an increase in the total drag coefficient. The total drag coefficient C_D is found to vary with $\sqrt{\beta}$ for $\beta \geqslant 2$. The linear dependence with $\sqrt{N}$ of drag coefficient is reported experimentally by Maxworthy [19], Yonas [20] and Josserand *et al.* [18]. There is a non-monotonic decrease in drag coefficient with R_m for low magnetic fields until $N \approx 1$ (Figure 15(c)). For higher interaction parameters, it decreases linearly with R_m.

DOI: 10.1002/fld

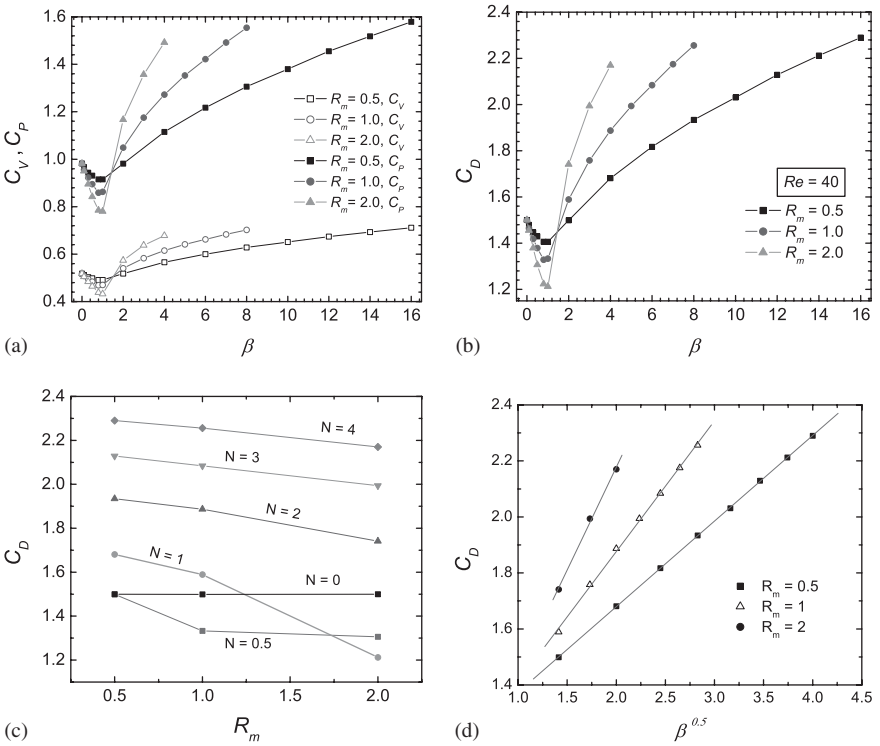

Figure 15. Variation of viscous drag coefficient C_V, pressure drag coefficient C_P, the total drag coefficient C_D as a function of β and the linear dependence of the drag coefficient with β.

5. CONCLUSIONS

In this paper, we have studied the control of flow separation using electromagnetic forces for different conductivities of the fluid. The separation for $Re=40$ is fully suppressed. The non-monotonic behavior that is observable under QS approximation in separation length and separation angle is not found. The separation for highly conducting fluids can be suppressed with low magnetic fields. The fluids with large conductivity have higher critical Reynolds number when compared with fluid flows without magnetic field. When $N<1$, the suppression of the flow-separation is nearly independent of the conductivity of the fluid, whereas for $N\geqslant 1$, the conductivity of the fluid strongly influences the control of flow-separation. The drag coefficient is found to decrease when $\beta\leqslant 1$ and it increases for higher values of β. It is found that C_P, C_D and the pressure coefficient at rear stagnation point $p(0,0)$ vary with $\sqrt{\beta}$ when $\beta>1$.

REFERENCES

1. McCune JE. On the motion of thin airfoils in fluid of finite electrical conductivity. *Journal of Fluid Mechanics* 1960; **7**:449–468.
2. Jang J, Lee SS. Theoretical and experimental study of mhd (magnetohydrodynamic) micropump. *Sensors and Actuators A* 2000; **80**:84–89.

DOI: 10.1002/fld

3. Tso CP, Sundaravadivelu K. Capillary flow between parallel plates in the presence of an electromagnetic field. *Journal of Physics D*: *Applied Physics* 2001; **34**:3522–3527.
4. Mutschke G, Gerbeth G, Shatrov V, Tomboulides A. The scenario of three-dimensional instabilities of the cylinder wake in an external magnetic field: a linear stability analysis. *Physics of Fluids* 2001; **13**:723–734.
5. Sekhar TVS, Sivakumar R, Ravi Kumar TVR. Drag and pressure fields for the MHD flow around a circular cylinder at intermediate Reynolds numbers. *Journal of Applied Mathematics* 2005; 183–203.
6. Sekhar TVS, Sivakumar R, Ravi Kumar TVR. Flow around a circular cylinder in an external magnetic field at high Reynolds numbers. *International Journal of Numerical Methods for Heat and Fluid Flow* 2006; **16**:740–759.
7. Sekhar TVS, Sivakumar R, Kumar H, Ravi Kumar TVR. Effect of aligned magnetic field on the steady viscous flow past a circular cylinder. *Applied Mathematical Modelling* 2007; **31**:130–139.
8. Poggie J, Gaitonde DV. Magnetic control of flow past a blunt body: numerical validation and exploration. *Physics of Fluids* 2002; **14**:1720.
9. Knaepen B, Kassinos S, Carati D. Magnetohydrodynamic turbulence at moderate magnetic Reynolds number. *Journal of Fluid Mechanics* 2004; **513**:199–220.
10. Ludford GSS. In *Magneto-fluid and Plasma Dynamics*, Grad H (ed.). American Mathematical Society: Providence, RI, 1967; 57.
11. Sarris IE, Zikos GK, Grecos AP, Vlachos NS. On the limits of validity of the low magnetic Reynolds number approximation in MHD natural-convection heat transfer. *Numerical Heat Transfer Part B*: *Fundamentals* 2006; **50**:157–180.
12. Ingham DB. Steady magnetohydrodynamic flow past a circular cylinder. *International Journal for Numerical Methods in Engineering* 1974; **8**:771–781.
13. Wesseling P. *An Introduction to Multigrid Methods*. R. T. Edwards Inc.: Philadelphia, U.S.A., 2004.
14. Juncu GH, Mihail R. Numerical solution of the steady incompressible Navier–Stokes equations for the flow past a sphere by a multigrid defect correction technique. *International Journal for Numerical Methods in Fluids* 1990; **11**:379–395.
15. Juncu Gh. Unsteady conjugate heat-mass transfer from a circular cylinder in laminar crossflow at low Reynolds numbers. *International Journal of Heat and Mass Transfer* 2004; **47**:2469–2480.
16. Juncu Gh. Unsteady forced convection heat/mass transfer from a flat plate. *Heat and Mass Transfer* 2005; **41**:1095–1102.
17. Maxworthy T. Experimental studies in magneto-fluid dynamics: flow over a sphere with a cylindrical afterbody. *Journal of Fluid Mechanics* 1969; **35**:411–416.
18. Josserand J, Marty Ph, Alemany A. Pressure and drag measurements on a cylinder in a liquid metal flow with an aligned magnetic field. *Fluid Dynamics Research* 1993; **11**:107–117.
19. Maxworthy T. Experimental studies in magneto-fluid dynamics: pressure distribution measurements around a sphere. *Journal of Fluid Mechanics* 1968; **31**:801–814.
20. Yonas G. Measurements of drag in a conducting fluid with an aligned magnetic field and large interaction parameter. *Journal of Fluid Mechanics* 1967; **30**:813–821.
21. Leibovich S. Magnetohydrodynamic flow at a rear stagnation point. *Journal of Fluid Mechanics* 1967; **29**:401–413.
22. Banks WHH, Zaturska MB. The flow of a electrically conducting fluid at a rear stagnation point. *Zeitschrift für Angewandte Mathematik und Physik* 1984; **35**:72–80.

DOI: 10.1002/fld